Journal of Materials Chemistry B

Accepted Manuscript

This article can be cited before page numbers have been issued, to do this please use: B. Thirumalraj, R. Chellakannu, S. CHEN and B. Palani, *J. Mater. Chem. B*, 2016, DOI: 10.1039/C6TB01576J.

ROYAL SOCIETY OF CHEMISTRY

www.rsc.org/materialsB

View Article Online
DOI: 10.1039/C6TB01576J

Highly stable biomolecule supported gold nanoparticles/graphene nanocomposite as a sensing platform for H_2O_2 biosensor application

Balamurugan Thirumalraj,[a] Chellakannu Rajkumar,[a] Shen-Ming Chen,[a*] and Palani Barathi [b]

[a]Department of Chemical Engineering and Biotechnology, National Taipei University of Technology, No.1, Section 3, Chung-Hsiao East Road, Taipei 106, Taiwan (ROC).

[b]Electrochemical Energy Research Lab, Centre for Nanoscience and Technology, Pondicherry University, Puducherry, 605014, India.

[*] Corresponding author. Fax: +886 2270 25238; Tel: +886 2270 17147
E-mail: smchen78@ms15.hinet.net

View Article Online
DOI: 10.1039/C6TB01576J

ABSTRACT

A highly active and stable hemin (HN) supported reduced graphene oxide/gold nanoparticles (HN-RGO/AuNPs) composite was prepared by one-pot hydrothermal method. The physicochemical properties of the as prepared composites were characterized by field emission scanning electron microscope (FESEM), transmission electron microscopy (TEM), UV-Vis spectroscopy, Raman spectroscopy and X-ray diffraction technique (XRD). The HN-RGO/AuNPs modified electrode shows a stable and well-defined surface confined redox couple at an apparent formal potential of –0.317 V vs. Ag|AgCl with a surface coverage value of 2.239 x 10^{-10} mol cm^{-2}. Compared with HN, HN-GO and HN-RGO, the HN-RGO/AuNPs modified electrode exhibits an excellent electrocatalytic activity towards hydrogen peroxide (H_2O_2). Under optimum conditions, the HN-RGO/AuNPs modified electrode shows a stable and wide linear response ranging from 0.05 μM to 518.15 μM towards H_2O_2 and fast response time (3 s). The calculated sensitivity and limit of detection (LOD) of the biosensor was 3.99 $\mu A \mu M^{-1}$ cm^{-2} and 16 nM, respectively. In addition, Michaelis-Menten constant value of the biosensor is 0.13 mM, which indicating the high affinity of HN towards the reduction of H_2O_2. The proposed biosensor displays a high sensitivity and selectivity towards H_2O_2 in presence of common biological co-existing species. The biosensor shows an acceptable practical ability in human serum, contact lens solution and milk samples with an appreciable recovery.

View Article Online
DOI: 10.1039/C6TB01576J

1. INTRODUCTION

To design and development of peroxidase-mimicking enzymes with an excellent catalytic activity and high substrate selectivity is much interest in analytical, biochemical and clinical chemistry due to the limitation of natural enzymes, which is used for the sensing of biological micro-molecules such as H_2O_2, glucose, dopamine, uric acid, ascorbic acid, and so on.[1,2] Hemin (HN) is an iron-containing porphyrin molecule which acts as an active center of protein family such as cytochrome, hemoglobin, myoglobin and peroxidase.[3] In particular, the direct electrochemistry of HN used as a model enzyme which can provide the mechanism for an electron transport in biological system and also it is commercially available, known structure, low cost and highly stable. The electron rich and planar structure of HN can be used as a peroxidase enzyme in electrocatalysis of small molecules related biological process,[4] which is made up of red blood cells processed from human blood and lowering the production of certain enzyme in our body. However, the direct application of HN have still challenges because of its molecular aggregation in aqueous solution to form dimmers and oxidative self-destruction in oxidizing media, which causes passivation of its catalytic activity.[5] In recent years, carbon nanomaterials have received much interest in research community due to its potential applications in various fields including sensors, batteries, electronic and so on.[6,7]

In particular, graphene or reduced graphene oxide (RGO) is a single layer 2D material which can be raised a much attention in electrochemical sensor and biosensor applications,[8–10] owing to its unique structural and superior properties such as large specific surface area, superior mechanical strength, high thermal and electrical conductivities etc.[11] The covalent and non-covalent interaction could be used for the functionalization of RGO sheets via the stacking interaction between RGO and other aromatic molecules such as HN, ascorbic acid or

View Article Online
DOI: 10.1039/C6TB01576J

tetrathiafulvalene under mild conditions.[12–14] On the other hand, the attractive electrocatalytic activity of metal nanoparticles were explored in different potential applications such as surface plasmonics, biosensor, diagnostics and catalysis.[15–18] Moreover, the noble metal nanoparticles are widely used as a sensitive probe for immobilization on graphene based biosensor to improve their catalytic activity and sensing performance.[19] In particular, gold nanoparticles (AuNPs) are extensively used for electron transfer reactions due to its higher surface area, good conductivity and biocompatibility.[20] Owing to its special properties, AuNPs can enhance the electron transfer between the redox centers and exhibits an exceptional electrocatalytic activity towards the reduction of H_2O_2. [21]

Hydrogen peroxide (H_2O_2) is a simplest peroxide, colorless liquid with bitter taste and plays an important role in biological system which is used for different potential applications such as pulp and paper bleaching industry, propellants in rockets, cleaning and disinfecting agents in domestic use, alternative medicine for emphysema, influenza and AIDS.[22,23] However, different nanomaterials have been constructed with peroxidase-like natural enzymes for electrocatalytic activity of H_2O_2 detection, which can instead of the peroxidase to oxidize H_2O_2 on the substrate.[1, 24] The possibility of incorporating HN with RGO through π-π interaction including hemin-graphene hybrid nanosheets,[25] heat treated hemin supported graphene,[26] hemin–graphene/poly(3,4-ethylenedioxythiophene) nanocomposite,[4] DNA/hemin/nafion–graphene, reduced graphene oxide/graphene sheets-hemin-Au nanoparticles,[27,28] hemin immobilized on chemically converted graphene [29] and graphite-single walled carbon nanotube-hemin[30] have been studied for the electrocatalytic activity of HN based biosensors for different applications. Many of these studies have some limitations and drawbacks such as less catalytic activity, poor redox features, selectivity and complicated preparation procedures. In particular, heat treated hemin-

View Article Online
DOI: 10.1039/C6TB01576J

graphene modified electrode showed poor redox signature [26] and hemin functionalized graphene oxide suffered from serious interference with ascorbic acid, dopamine and uric acid.[31] More recently, Gu et al., reported a reduced graphene oxide-Hemin-Au nanohybrids for H_2O_2 sensor, which shows a poor sensitivity and lower liner range.[27] However, compared with previous report, our developed biosensor exhibited a very excellent electrocatalytic activity and higher sensitivity with wide linear response towards the reduction of H_2O_2.

In this study, we report a one-pot synthesis of HN functionalized reduced graphene oxide/gold nanoparticles (HN-RGO/AuNPs) composite which was prepared by a simple hydrothermal method. The HN-RGO/AuNPs modified electrode showed a well-defined redox couple and higher electrocatalytic activity than the HN, HN-GO, HN-RGO modified electrodes. The electrocatalytic activity and sensing performance of HN-RGO/AuNPs shows much higher than that of previously reported hemin based H_2O_2 biosensors. Based on this, we report a highly active and stable HN-RGO/AuNPs composite for sensitive and selective electrochemical detection of H_2O_2. The selectivity, higher stability and practicality of the proposed biosensor has also been crucially accessed and established. The biosensor was used for the determination of H_2O_2 level in human blood serum, contact lens solution and milk samples for practical applications.

2. Experimental

2.1. Materials

Hemin (BioXtra, from Porcine, ≥ 98%) and chloroauric acid ($HAuCl_4.3H_2O$, ≥ 49.0% Au basis) were supplied from Sigma-Aldrich used without further purification. Glucose and 30% ammonium hydroxide (NH_4OH) solution were obtained from Sigma-Aldrich. Contact lens (containing 3% H_2O_2) solution was purchased from China Chemical and Pharmaceutical, Taipei, Taiwan. Human blood serum sample was collected from valley biomedical, Taiwan product &

View Article Online
DOI: 10.1039/C6TB01576J

services, Inc. The supporting electrolyte was prepared by using 0.05 M disodium hydrogen phosphate (Na_2HPO_4) and sodium dihydrogen phosphate (NaH_2PO_4) solutions in doubly distilled water. All other chemicals were of analytical grade and all solutions were prepared using doubly distilled water without any further purification.

2.2. Instrumentation

Cyclic voltammetry (CV) and amperometry *i-t* measurements were carried out using CHI 1205b computerized electrochemical work station. The surface morphologies of the prepared composites were characterized by field emission scanning electron microscope (FE-SEM) using HitachiS-3000H scanning electron microscope and the elemental mapping was performed by HORIBA EMAX X-ACT attached with HitachiS-3000H microscope and high resolution-transmission electron microscopy (HR-TEM, JEOL, JEM-3000F) operated at 300 kV. Ultraviolet-visible (UV-Vis) spectra and Raman spectrum were performed using Hitachi U-3300 UV spectrophotometer and Dong Woo 500i, Korea equipped with a 50× objective and a charge-coupled detector respectively. The X-ray diffraction (XRD) pattern was taken by using XPERT-PRO (PANalytical B.V., The Netherlands) diffractometer (Cu Kα radiation, k = 1.54 Å). A conventional three electrode system with glassy carbon electrode (GCE) as a working electrode; Ag/AgCl (in saturated KCl) as a reference electrode; and platinum wire as a counter electrode were used in this work.

2.3. Synthesis of HN-RGO/AuNPs composite

The one-pot synthesis of HN-RGO/AuNPs composite was prepared by hydrothermal method. First, graphene oxide (GO) was synthesized using modified Hummers' method.[32] The HN-RGO/AuNPs composite was prepared as follows. Typically, the homogenous dispersion of GO (0.5 mg/mL) was mixed with HN solution (1 mg/mL ethanol) followed by the addition of

View Article Online
DOI: 10.1039/C6TB01576J

NH_4OH solution (pH 9-10), the mixture gets dark reddish brown. The reaction mixture was stirred for 1 h to allow the interaction between hemin moiety and GO sheets. Then, $HAuCl_4$ (0.5 mM) was added into the solution and vigorously stirred for 30 min. After that, the aqueous solutions were mixed together and reduced to HN-RGO and AuNPs by adding glucose (0.1 M) into the solution. The reaction mixture was heated to 95 °C and stirred vigorously for 2 h. After completing the process, the reaction mixture was allowed to cool to room temperature. The resulting black HN-RGO/AuNPs nanocomposite was centrifuged at 6000 rpm to remove the unreacted particles in HN-RGO/AuNPs composite. Finally, the composite was washed with DI water and ethanol, dried at 50 °C for 6 h and it could be dispersed in DI water by ultrasonication.

2.4. Fabrication of HN-RGO/AuNPs modified electrode

Prior to use, mirror like GCE was polished with 0.05 μM alumina slurry and washed thoroughly with DI water and ethanol for each polishing using ultra sonication and dried in hot air oven. About 8 μL of HN-RGO/AuNPs composite was drop casted on the pre-cleaned GCE and allowed to dry in N_2 atmosphere. The HN-RGO/AuNPs composite modified GCE was used for further electrochemical experiments and kept in room temperature when not in use. Similarly, the absence of AuNPs in HN-GO/GCE and HN-RGO/GCE composites were prepared for comparison studies. All other electrochemical experiments were carried out in N_2 atmosphere. The preparation of HN-RGO/AuNPs composite and electrochemical pathway of H_2O_2 reduction is shown in **scheme 1**.

View Article Online
DOI: 10.1039/C6TB01576J

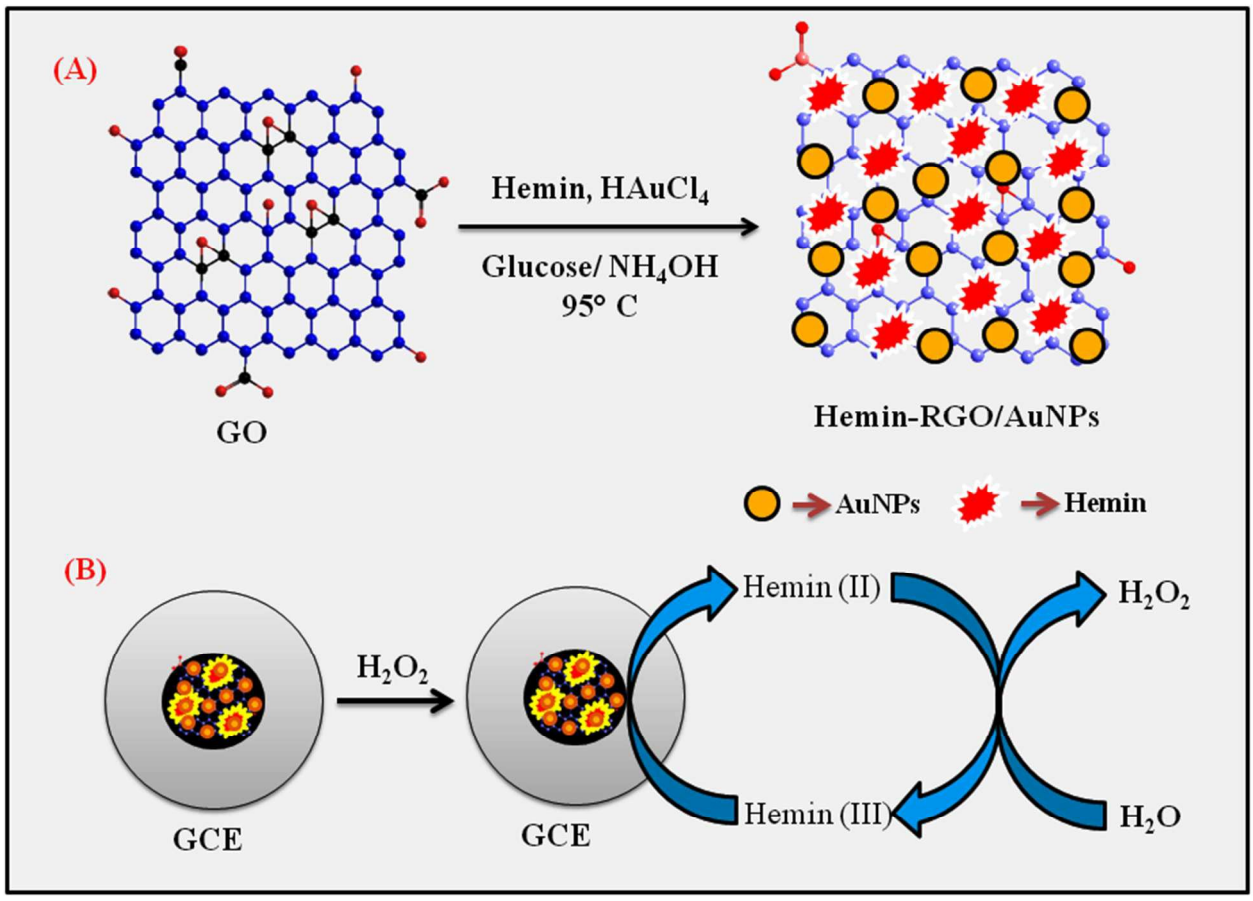

Scheme 1 Schematic representation for the preparation of HN-RGO/AuNPs composite (A) and (B) Electrochemical pathway for H_2O_2 reduction.

3. Results and discussion

3.1. Characterization of HN-RGO/AuNPs composite

The surface morphologies of GO, HN, HN-RGO and HN-RGO/AuNPs composites were characterized by FESEM. The typical FESEM images of GO (A), HN (B), HN-RGO (C) and HN-RGO/AuNPs (D) composite are shown in Fig.S1. The SEM image of GO (Fig.S1A) shows an ultra wrinkled thin film like structure which confirms the GO sheets are assembled layer-by-layer and the SEM image of HN (Fig.S1B) reveal that a rod-like morphology. On the other hand, HN-RGO (Fig.S1C) composite shows a crumbled morphology which is further confirms the hemin moieties were tightly aggregated on RGO surface through strong π-π interaction, which

View Article Online
DOI: 10.1039/C6TB01576J

indicating the higher surface area of HN-RGO. However, the HN-RGO/AuNPs (Fig.S1D) composite, we could be observed that a small tiny and nano sized particles were homogeneously grown on HN-RGO surface, which indicating the presence of AuNPs were successfully intercalated on HN-RGO surface. The prepared HN-RGO/AuNPs composite was further confirmed by TEM images as shown in Fig.1. It can be seen that the nano sized small AuNPs are uniformly covered on the surface of HN-RGO layer. The average diameter of AuNPs on HN-RGO surface was 68±5 nm (observed from **Fig.1**). In addition, the EDX elemental mapping also supports the formation of AuNPs on HN-RGO surface. The SEM image of HN-RGO/AuNPs (A) composite and corresponding elemental mapping of carbon (B), oxygen (C) and gold (D) nanoparticles, results are shown in **Fig.S2**.

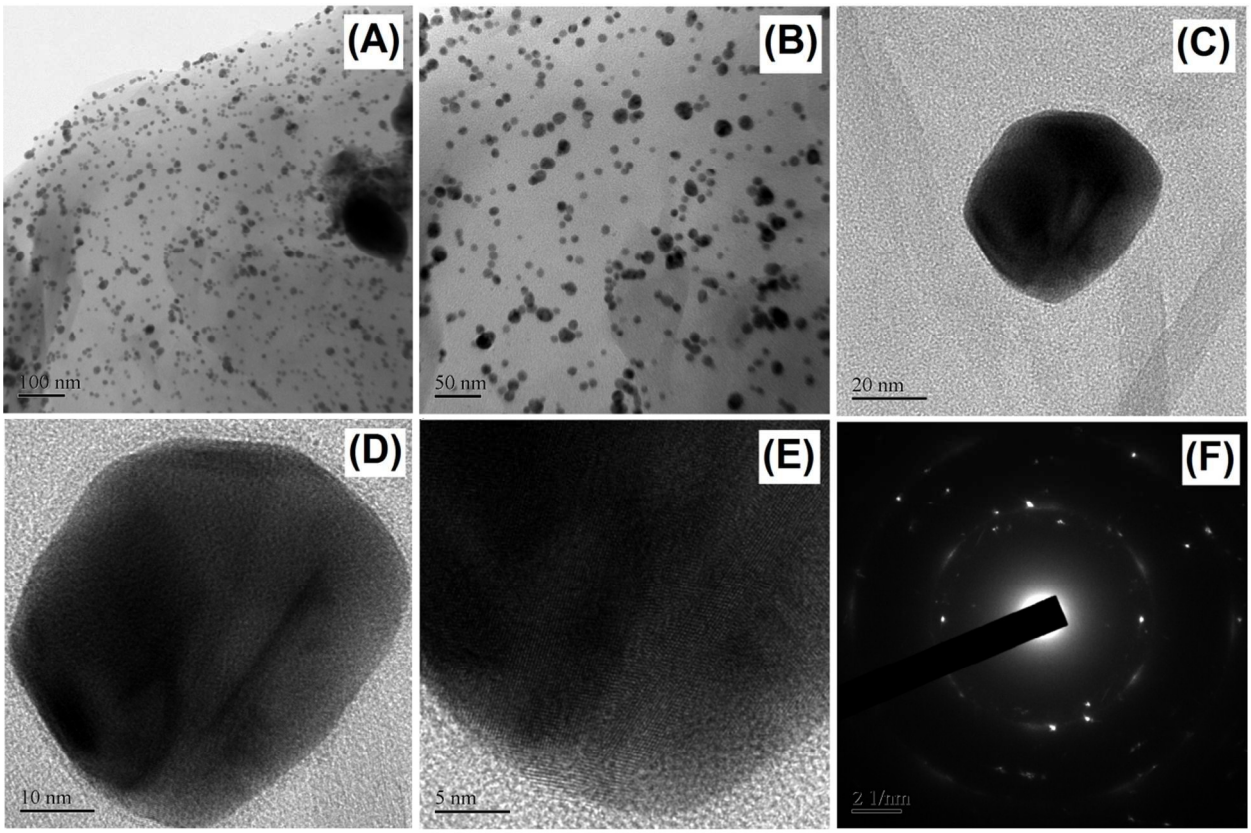

View Article Online
DOI: 10.1039/C6TB01576J

Fig. 1 HR-TEM images of HN-RGO/AuNPs with different magnifications (A-E) and (F) corresponding SEAD diffraction pattern of AuNPs.

The HN-RGO/AuNPs composite was further characterized by UV–vis spectroscopy. As shown in Fig.2A, GO (a) exhibits a maximum absorption peak at 235 nm which is the π-π* transition of aromatic C=C bonds and a shoulder peak at about 300 nm belongs to the n-π* transition of C=O.[33] On the other hand, HN (b) shows a typical Soret absorption band at 387 nm and also a series of weak absorption band occurs at longer wavelengths between 500–700 nm, which indicating the presence Q-bands of HN moiety . The HN-RGO (c) composite displays two strong absorption peaks at 267 and 423 nm with a large bathochromic shift, which is due to interaction between porphyrin moiety of HN and RGO through π–π stacking interactions to further confirm the formation of HN-RGO. In addition, a new absorption peak at 539 nm which is corresponding to the surface Plasmon absorption of AuNPs on HN-RGO surface. This result clearly indicates that the formation of AuNPs is homogeneously decorated on HN-RGO surface.

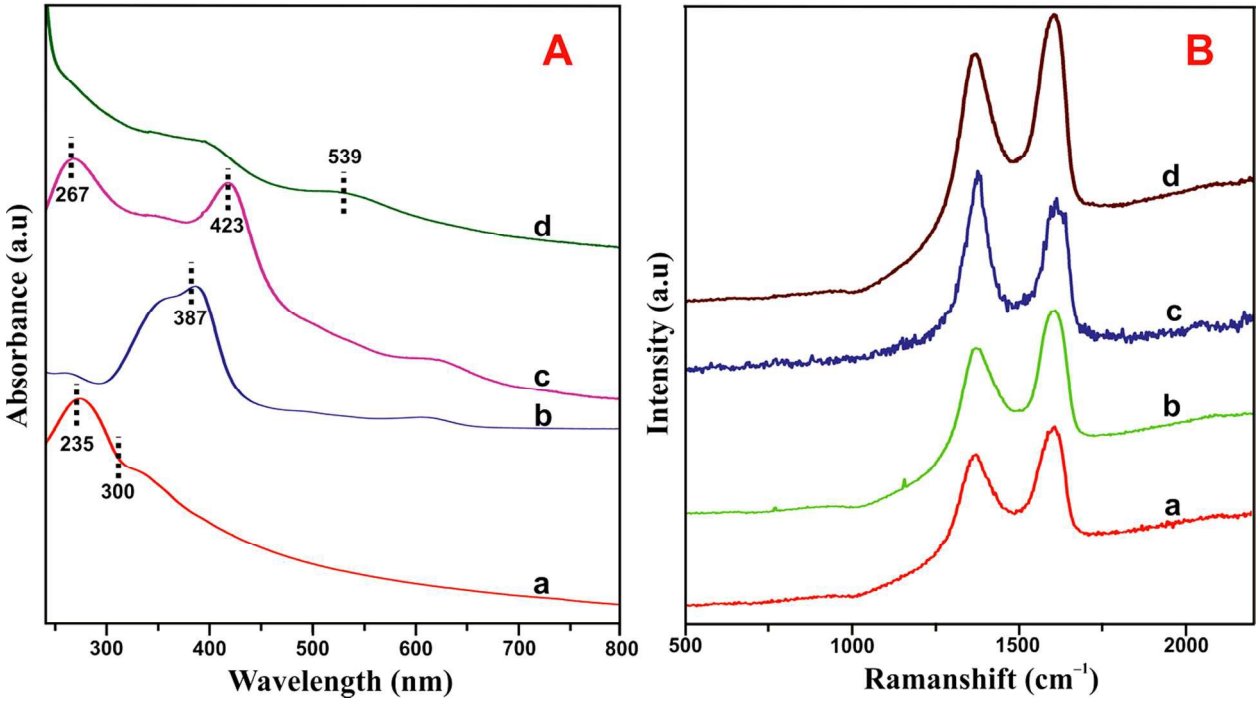

View Article Online
DOI: 10.1039/C6TB01576J

Fig. 2 (A) UV-Vis spectra of GO (a), HN (b), HN-RGO (c) and HN-RGO/AuNPs (d) composite. (B) Raman spectra of GO (a), HN-GO (b), HN-RGO (c), HN-RGO/AuNPs (d) composite.

The crystalline nature of graphene and hybrid nanomaterials were characterized by Raman spectroscopy. Fig.2B depicts the Raman spectra of GO (a), HN-GO (b), HN-RGO (c) and HN-RGO/AuNPs (d) composite. It can be clearly seen that GO shows two specific peaks at a frequencies of 1570 and 1330 cm^{-1}, which is corresponding to the sp^2 carbon in pure graphite structure (G band) and sp^3 carbon units of defects and disordered oxygen functionalities (D band), respectively.[34,35] The calculated intensity ratio (I_D/I_G) values for GO, HN-GO, HN-RGO and HN-RGO/AuNPs composites were 0.879, 1.221, 1.37 and 1.402, respectively. The I_D/I_G value of HN-RGO/AuNPs composite is much higher than that of GO, HN-GO, HN-RGO which is also confirms the formation of strong π–π interaction between the porphyrin units of HN and graphitic units of RGO/AuNPs. This results confirms that the formation of GO to RGO and the HN molecules are successfully attached to the surface of RGO.

The HN-RGO/AuNPs composite was further confirmed by XRD pattern. Fig.S3 shows the XRD patterns for GO (a), HN-RGO (b) and HN-RGO/AuNPs (c) composite. It can be seen that GO shows two discrete 2θ peaks at 11.52 and 26.68° apart from the 2θ peaks of ITO (21.46, 30.32, 35.12, 50.34 and 60.22°).The specific peaks are analogous to a report by Hae et al. for the hydroxyl, epoxide, and carboxyl functionalized GO.[36] According to JCPDS no.01-088-0315, the cubic crystalline Fe_2O_3 show two sharp peaks at 30.32° and 35.58° which indicating the presence of HN due to the oxidation of Fe in HN by the trace dioxygen in the atmosphere.[37] In addition compared with GO and HN-RGO composite, there are two diffraction peaks were observed in HN-RGO/AuNPs which could be indexed to (111), (200) planes of AuNPs as per the JCPDS file for the bulk Au,[38] which is strongly indicating the presence of HN is strongly attached to RGO and the AuNPs are decorated on HN-RGO surface.

View Article Online
DOI: 10.1039/C6TB01576J

3.2 Electrochemical behavior of HN-RGO/AuNPs modified electrode

The electrochemical behavior of HN modified different electrodes were investigated by CV. Fig.3(A) shows the CV response of HN (a), HN-GO (b), HN-RGO (c) and HN-RGO/AuNPs (d) modified electrodes in N_2 saturated PBS at a scan rate of 100 mVs^{-1}. It can be seen that there is a weak quasi-reversible redox peak was observed at HN (a) modified electrode. The HN-GO (b) modified electrode showed a weak redox peak was observed, while a cathodic and anodic peak appeared at –0.392 and –0.321 V, respectively.

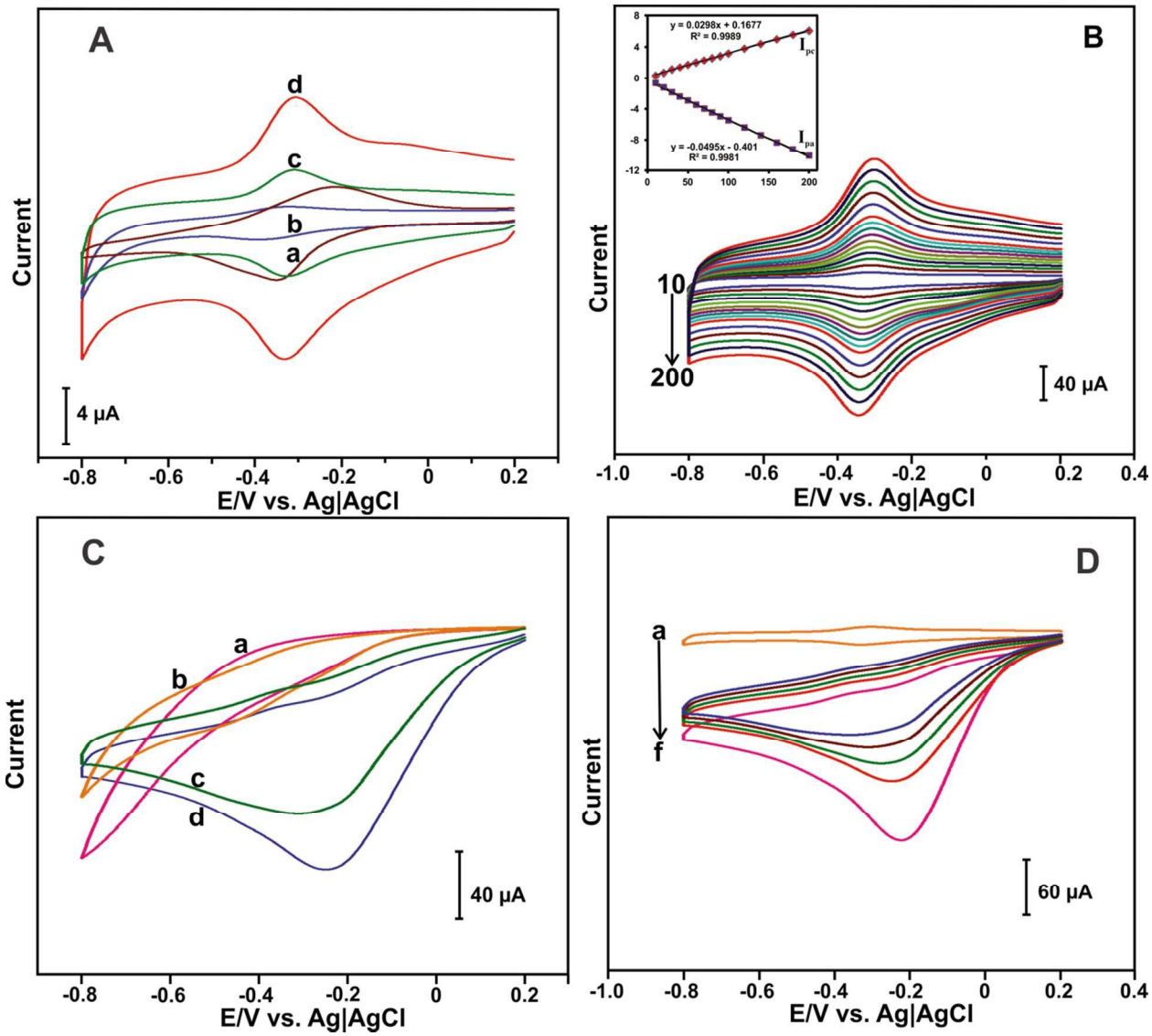

View Article Online
DOI: 10.1039/C6TB01576J

Fig. 3 (A) CV response of HN (a), HN-GO (b), HN-RGO (c) and HN-RGO/AuNPs (d) modified electrodes in N_2 saturated PBS at a scan rate of 100 mVs^{-1}. (B) CV response of HN-RGO/AuNPs modified electrode in N_2 saturated PBS at a scan rates from 10–200 mVs^{-1}. The corresponding calibration plot for I_{pa} and I_{pc} vs. scan rate. (C) CV curves of HN (a), HN-GO (b), HN-RGO (c) and HN-RGO/AuNPs (d) modified electrodes in 50 μM H_2O_2 containing N_2 saturated PBS at a scan rate of 100 mVs^{-1}. (D) CV curves of HN-RGO/AuNPs modified electrode in the absence (a) and presence of different additions of H_2O_2 (10 μM (b–e), 20 μM (f)) in N_2 saturated PBS at a scan rate of 100 mVs^{-1}.

On the other hand, the HN-RGO (c) modified electrode showed a well defined redox couple was observed, whereas the cathodic and anodic peaks were located at –0.331 and –0.308 V, respectively. Compared with HN, HN-GO and H-RGO modified electrodes, the HN-RGO/AuNPs modified electrode showed a stable and well defined redox couple [Hemin Fe(III)↔Hb Fe(II)] with a formal potential (E°) of –0.317 V, while the peak to peak separation (ΔE_p) value of 21 mV which was much lower than other HN modified electrodes as reported early,[39] which indicating fast electron transfer of HN on the electrode surface.[40] The fast electron transfer and excellent electrochemical behavior of HN shows its good biocompatibility in RGO/AuNPs, suggests that the presence of AuNPs can enhance the electron transfer behavior of HN on the electrode surface.

To investigate the electrochemical behavior of HN-RGO/AuNPs modified electrode at different scan rates was performed by CV. Fig.3(B) shows the CV response of HN-RGO/AuNPs modified electrode in N_2 saturated PBS at different scan rates from 10–200 mVs^{-1}. It can be seen that the redox couple of anodic (I_{pa}) and cathodic (I_{pc}) peak current was gradually increased upon increasing the scan rate. The calibration plot of I_{pa} and I_{pc} has a linear dependence over the scan rate from 10 to 200 mV s^{-1} with a correlation coefficient of I_{pa} and I_{pc} is 0.9981 and 0.9989, respectively (Fig.3B Inset). The result further confirmed that the redox electrochemical behavior

View Article Online
DOI: 10.1039/C6TB01576J

of HN on HN-RGO/AuNPs modified electrode was embedded by surface controlled process.[41] The average surface coverage value of HN on HN-RGO/AuNPs modified electrode can be calculated using the following equation (1).

$$\Gamma = Q/nFA \qquad \ldots\ldots. (1)$$

Where, "Q" is the total charge (Q = 5.619 μC), "n" is the number of electrons involved in electron transfer processes (n = 1), "F" is Faraday's constant (96485.34 C mol^{-1}) and "A" is geometric area of the electrode (0.26 cm^2). From the above equation, calculated Γ value was found to be 2.239 x 10^{-10} mol cm^{-2} which was much higher than that of previously reported theoretical mono layer coverage of HN modified electrode.[42] The larger surface coverage value reveals that the HN was strongly immobilized on RGO/AuNPs surface, which can enhance the electrochemical activity and higher stability on the electrode surface.

To further investigate the electrochemical behavior of HN-RGO/AuNPs modified electrode on different pH was studied by CV. The protonation of heme ions depending on the pH solution. Besides, the electrochemical behavior of enzymatic biosensors generally affects the pH solution. Hence, we have studied the effect of pH solution using HN-RGO/AuNPs modified electrode. Fig.S4(A) depicts the CV response obtained at HN-RGO/AuNPs modified electrode in N_2 saturated different pH solutions (3, 5, 7, 9 and11) at a scan rate of 100 mVs^{-1}. A well-defined redox couple was observed for each pH. The peak potential (E_{pa} and E_{pc}) was shifted toward positive and negative directions upon increasing and decreasing the pH. The calibration plot of E° vs. pH showed a linear dependence with a slope and correlation coefficient of −52.6 mV/pH and 0.9933 respectively and the results are shown in Fig.S4(B), which indicating the redox electrochemical redox behavior of HN participating equal number of proton (H^+) and electron (e^-) in the electrochemical process.

View Article Online
DOI: 10.1039/C6TB01576J

3.3 Electrocatalytic reduction of H_2O_2 at HN-RGO/AuNPs modified electrode

To investigate the electrocatalytic activity of HN-RGO/AuNPs modified electrode toward H_2O_2 reduction was performed by CV. The CV curves of HN (a), HN-GO (b), HN-RGO (c) and HN-RGO/AuNPs (d) modified electrodes containing 50 μM H_2O_2 in PBS at a scan rate of 100 mVs^{-1}, are shown in Fig.3C. It can be seen that there is no obvious reduction peak was observed in presence of 50 μM H_2O_2 at HN and HN-GO modified electrodes. While, a weak cathodic peak was observed at –0.23 V in the presence of 50 μM H_2O_2 at HN-RGO modified electrode, which indicating a typical electrocatalytic reduction of H_2O_2. However, a sharp cathodic peak was observed at –0.18 V on HN-RGO/AuNPs modified electrode, which suggests that the after introducing the AuNPs on HN-RGO can enhance the electrocatalytic activity of H_2O_2, mediated by Fe^{3+}/Fe^{2+} (HN) on the electrode surface. In addition, we have studied the effect of AuNPs on HN-RGO/AuNPs composite formation for the detection of H_2O_2 using different concentrations of $AuCl_4.3H_2O$ solution and the results are shown in Fig.S5. It can be seen that the higher response current of H_2O_2 was observed in 0.5 mM $AuCl_4$ solution on HN-RGO/AuNPs composite. However, the response current was rapidly decreased while increasing or decreasing the $AuCl_4$ concentration. Hence, 0.5 mM of $AuCl_4$ solution is an optimum concentration on HN-RGO/AuNPs with an average diameter of AuNPs is 68±5 nm (see Fig.1). Moreover, the electrocatalytic activity of HN-RGO/AuNPs modified electrode towards different additions of H_2O_2 was studied by CV. As shown from Fig.3(D), the CV response obtained at HN-RGO/AuNPs modified electrode in the absence (a) and presence of different addition of H_2O_2 in PBS at a scan rate of 100 mVs^{-1}. We could observed that well-defined redox couple was observed at HN-RGO/AuNPs modified electrode in the absence of H_2O_2.Noticeably, the cathodic peak current gradually increases with increasing concentration of H_2O_2 (10 μM (b–e),

View Article Online
DOI: 10.1039/C6TB01576J

20 μM (f)) and the anodic peak was decreases gradually, which reveals that the HN-RGO/AuNPs modified electrode has higher electrocatalytic activity towards H_2O_2.This result suggests that the HN-RGO/AuNPs modified electrode exhibits fast electron transfer and higher electrocatalytic activity towards the reduction of H_2O_2.

3.4 Amperometric determination of H_2O_2

An accurate and low level determination of H_2O_2 using HN-RGO/AuNPs modified rotational disk electrode (RDE) was evaluated by amperometric method. Fig.4(A) shows an amperometric *i-t* response of HN-RGO/AuNPs modified RDE for the successive additions of different concentration of H_2O_2 into N_2 saturated constantly stirred PBS at an applied potential of –0.18 V. As seen from Fig.4A, a well defined and stable amperometric response was observed for different additions of H_2O_2 at HN-RGO/AuNPs modified RDE and reached a stable current within 3s, which indicating fast electron transfer on the electrode surface and higher electrocatalytic activity towards H_2O_2 reduction. The response current of the biosensor had linear dependent over the concentrations of H_2O_2 ranging from 0.05 to 518.15 μM with a sensitivity of 3.99 $\mu A \mu M^{-1} cm^{-2}$ (Fig.4B). The limit of detection (LOD) was calculated as 16 nM based on *S/N*=3.[43] The efficiency of the proposed biosensor was compared with previously reported HN based biosensors. However, various metal nanoparticles are used for non enzymatic H_2O_2 sensor. Hence, it is necessary to compare the analytical performance of the proposed biosensor with previous studies and the results are shown in Table 1.[4,25,27,28,30,50–56]

View Article Online
DOI: 10.1039/C6TB01576J

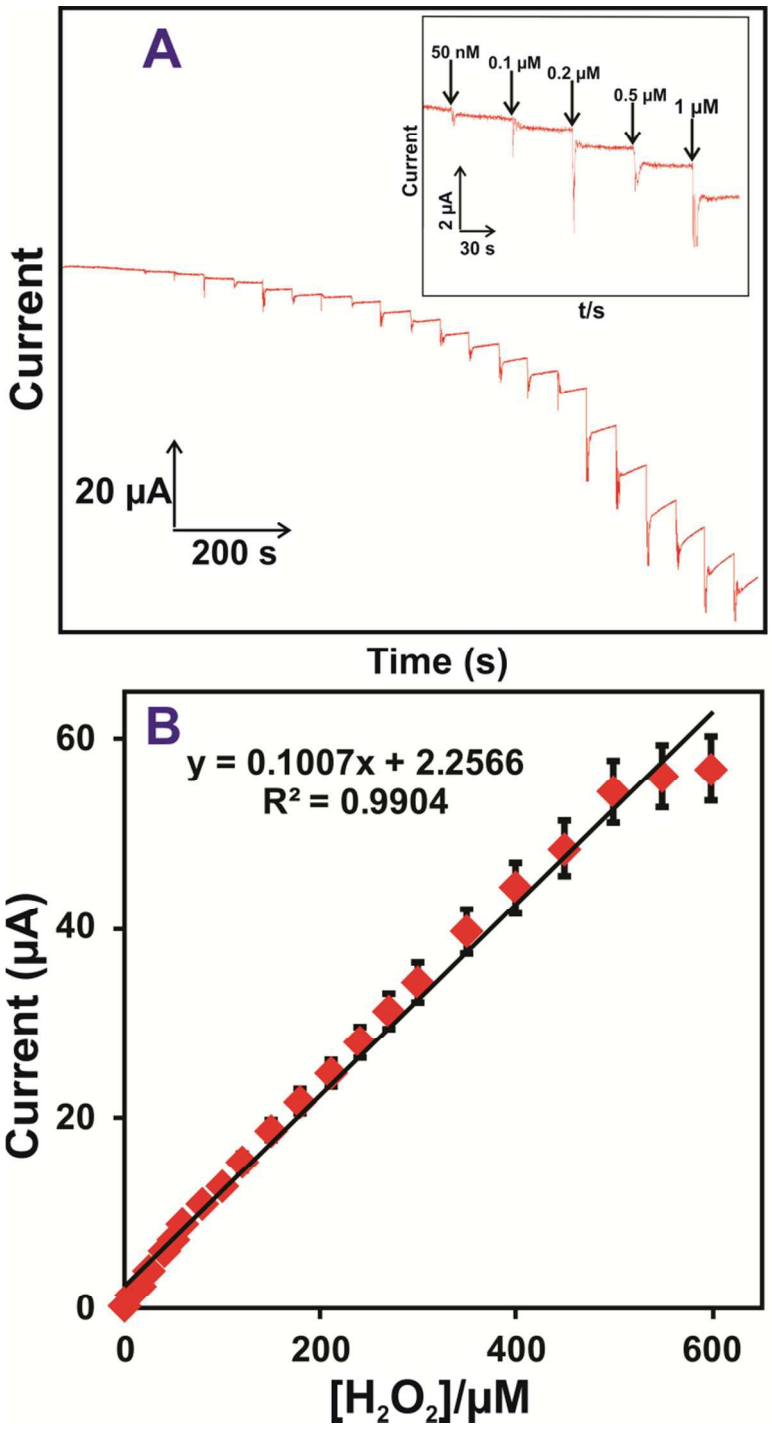

Fig. 4 (A) Amperometric *i-t* response for HN-RGO/AuNPs modified RDE for the successive additions of different concentration of H_2O_2 into N_2 saturated constantly stirred PBS at an applied potential of –0.18 V. Inset: enlarged view of Fig 4A. (B) Calibration plot for cathodic peak current vs. $[H_2O_2]$ and the error bar indicates the standard deviation of three measurements.

View Article Online
DOI: 10.1039/C6TB01576J

Moreover, the resultant current was deviated linearly towards H_2O_2 concentrations (Fig.4B), which revealed that the kinetics of electrocatalytic process was followed by Michaelis–Menten (MM) model. The possible mechanism for MM reaction pathway for H_2O_2 is given below.[44–46]

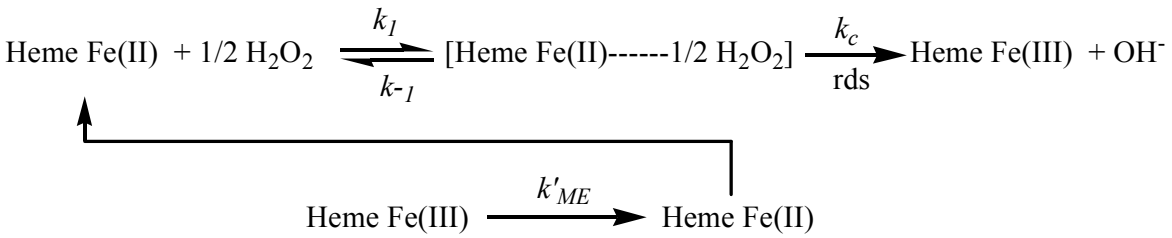

Where k_M = apparent MM rate constant ($(k_{-1} + k_c)/k_1$), k_c = first order chemical rate constant and k'_{ME} = heterogeneous modified electrode rate constant. The calculated values are k_M= 0.13 mM, kc = 29.7/s, and k'_{ME} = 0.0183 cm/s, respectively. Compared with some enzymatic and HN based biosensor, the calculated K_M value of HN-RGO/AuNPs modified electrode is much smaller than that of cytochrome c immobilized macro electrode of 1.38 mM,[47] Hb immobilized impure multiwalled carbon nanotube modified electrode of 2 mM,[48] RGO-Au-Hemin composite of 3.1 mM [49] and hemin-graphene hybrid Nanosheets of 2.256 mM.[24] This result suggests that HN-RGO/AuNPs modified electrode has good biological affinity and higher biocatalytic activity towards the reduction of H_2O_2.

3.5 Selectivity, stability, repeatability and reproducibility

The selectivity, stability, repeatability and reproducibility of the H_2O_2 biosensor are more important for practical applications. Fig.5(A) depicts the amperometric *i-t* responses obtained at HN-RGO/AuNPs modified RDE for the successive addition of 5 μM H_2O_2 (a), 100 μM of DA (b), AA (c), UA (d), melatonin (e), EP (f), NEP (g) and glucose (h) into constantly stirred N_2 saturated PBS at –0.18 V.

View Article Online
DOI: 10.1039/C6TB01576J

Table 1. Comparison of analytical performance of HN-RGO/AuNPs modified electrode with previously reported HN based biosensor and metal based non-enzymatic H_2O_2 biosensor.

Modified electrodes	Detection Limit (μM)	Applied potential (V) vs. Ag|AgCl	Linear range (μM)	Ref.
Hemin-graphene-PEDOT/GCE	0.08	– 0.2	0.5–70	4
Hemin-GNs/GCE	0.20	– 0.2	0.5–400	25
RGO-Hemin-Au/GCE	0.03	– 0.18	0.1–40	27
Hemin-GNs-AuNPs/GCE	0.11	– 0.2	0.3–1800	28
GN-Hemin-SWCNT/GCE	0.05	– 0.2	0.2–400	30
Hemin-OMC-Nafion/GCE		– 0.4	2–250	50
PPY-Hemin-RGO/GCE	0.13	– 0.15	0.5–80	51
AgNPs/PANINFs/GCE	1.7	–0.3	100–60000	52
AuPs/GCE	4.0	–0.3	100–50000	53
AgNPs-RGO/GCE	1.8	–0.3	100–60000	54
AgNP-PPyC/GCE	1.05	–0.3	100–90000	55
Ag/GN/GCE	28	–0.4	100–40000	56
HN-RGO/AuNPs/GCE	0.016	– 0.18	0.05–518.15	This work

Abbreviations: GNs – graphene nanosheets, OMC – ordered mesoporous carbon, PPY– polypyrrole, PEDOT – poly(3,4-dioxyetylenethionphene), SWCNT – single–walled cabon nanotube, AuNPs– gold nanoparticles, RGO – reduced graphene oxide, GCE – glassy carbon electrode, AgNPs – silver nanoparticles, PANINFs – polyaniline nanofibers, AuPs – gold nanoplates, PPyC – polypyrrole colloids.

View Article Online
DOI: 10.1039/C6TB01576J

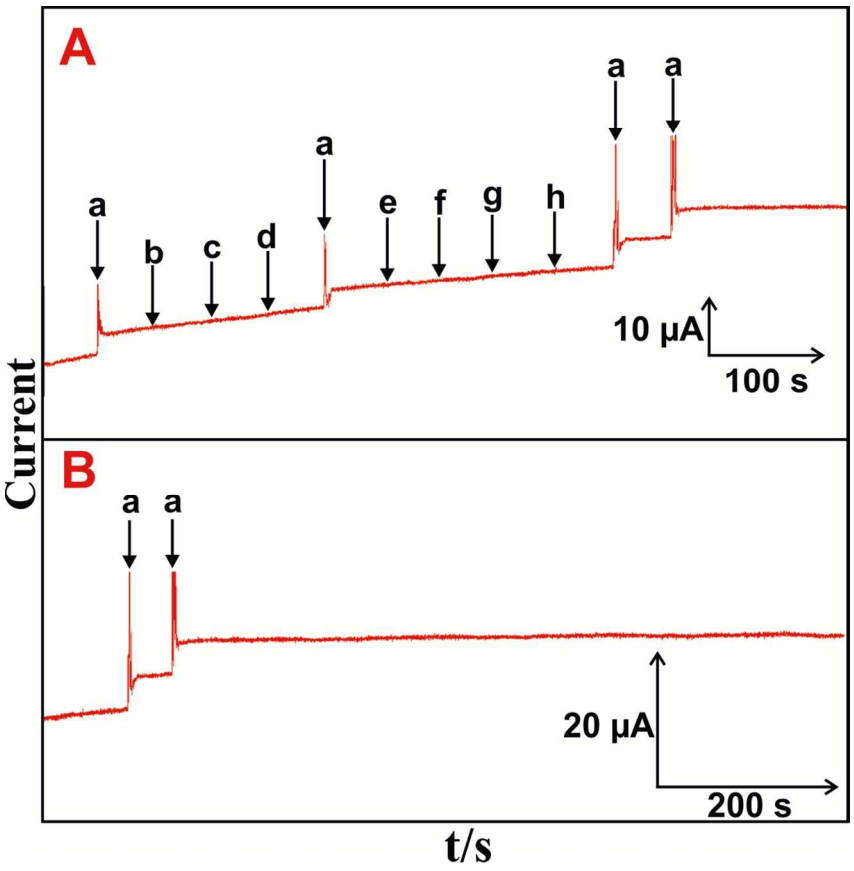

Fig.5 (A) Amperometric *i-t* response for HN-RGO/AuNPs modified RDE for the addition of 5 μM H_2O_2 (a), 100 μM of DA (b), AA (c), UA (d), melatonin (e), EP (f), NEP (g) and glucose (h) into constantly stirred N_2 saturated PBS. (B) Amperometric *i-t* response for HN-RGO/AuNPs modified RDE for the addition of 5 μM (a) into N_2 saturated constantly stirred PBS up to 1800 s.

It can be noted that a stable and sharp amperometric response current was observed for the addition of 5 μM H_2O_2, while no obvious response was observed for H_2O_2 with a sequential addition of above mentioned biological interfering species, which suggests that the biosensor was highly active and selective detection of H_2O_2. Moreover, the CV response for continuous cycling (n=25) of HN-RGO/AuNPs modified electrode in N_2 saturated PBS at a scan rate of 100 mVs^{-1}. It can be seen that there no change in the redox behavior and did not show any alternate change in peak current and peak potential (figure not shown), implying an appreciable stability of HN-RGO/AuNPs. The operational stability of HN-RGO/AuNPs modified RDE for 5 μM

View Article Online
DOI: 10.1039/C6TB01576J

H_2O_2 was investigated by amperometry and the results are shown in Fig.5(B). The other experimental conditions are similar as shown in Fig.4A. The biosensor retains 98.9 % of its initial amperometric response for the addition of 5 μM H_2O_2 containing N_2 saturated constantly stirred in PBS up to 1800 s. The results validate that higher operational stability of the biosensor towards H_2O_2. The repeatability of the biosensor was evaluated for determination H_2O_2 with a relative standard deviation (RSD) of 2.8% for 10 successive measurements. This result suggests that HN-RGO/AuNPs modified electrode exhibits a highly stable and sensitive detection of H_2O_2 for practical applications.

Table 2 Determination of H_2O_2 in Human serum, contact lens solution and milk samples using HN-RGO/AuNPs composite modified electrode (n=3).

Sample	Spiked (μM)	Found (μM)	Recovery (%)	RSD (%)
Human serum	0.5	0.47	94.0	2.6
	0.5	0.49	98.0	2.8
Contact lens solution	0.5	0.49	98.0	3.2
	0.5	0.51	102.0	3.4
Milk sample	0.5	0.53	106.0	3.9
	0.5	0.51	102.0	3.7

3.6 Real sample analysis

The practical ability of the biosensor was studied in real sample analysis using amperometry. The human blood serum, contact lens solution and milk samples containing H_2O_2 were tested by standard addition method. The samples were diluted with PBS and the known

View Article Online
DOI: 10.1039/C6TB01576J

concentration of H_2O_2 containing samples were spiked into PBS. The experimental conditions are similar in Fig.4A. The recovery values are shown in Table 2. The recovery values are retains approximately 100 %. This result authenticates that the proposed biosensor has good practicality for the detection of H_2O_2 in real sample analysis for biological applications.

4. CONCLUSIONS

In conclusion, we reported a one-pot synthesis of highly stable biomolecule supported HN-RGO/AuNPs composite for high performance H_2O_2 biosensor. The HN-RGO/AuNPs modified electrode showed excellent electrocatalytic activity such as higher sensitivity, stability, fast response towards the reduction of H_2O_2 than that of other HN modified electrodes. The biosensor exhibited excellent amperometric response towards H_2O_2 in PBS with common interfering biological molecules such as a DA, AA, UA, melatonin, EP, NEP and glucose. The electrochemical results suggested the biosensor has higher sensitivity, stability and lower LOD (16 nM) towards H_2O_2. We have successfully demonstrated the detection of H_2O_2 in real sample analysis with good average recovery of ~100%. As a future perspective, we believe that the biosensor could be used for biomedical, biological and electronic biosensor devices.

ACKNOWLEDGEMENTS

This project was supported by Ministry of Science and Technology (NSC101-2113-M-027-001-MY3), Taiwan. (Republic of China).

View Article Online
DOI: 10.1039/C6TB01576J

REFERENCES

1 H. Wei and E. Wang, *Anal. Chem*., 2008, **80**, 2250 – 2254.

2 T. Xue, S. Jiang, Y. Qu, Q. Su, R. Cheng, S. Dubin, C. Y. Chiu, R. Kaner, Y. Huang and X. Duan, *Angew. Chem. Int. Ed. Engl.,* 2012, **51**, 3822–3825.

3 Z. Genfa, and P. K. Dasgupta, *Anal. Chem*., 1992, **64**, 517–522.

4 W. Lei, L. Wu, W. Huang, Q. Hao, Y. Zhang and X. Xia, *J. Mater. Chem. B,* 2014, **2**, 4324–4330.

5 F. T. Zhang, X. Long, D. W. Zhang, Y. L. Sun, Y.L. Zhou, Y.R. Ma, L. M. Qi and X. X. Zhang, *Sens. Actuators, B,* 2014, **192**, 150–156.

6 T. Kuila, A. K. Mishra, P. Khanra, N. H. Kim and J. H. Lee, *Nanoscale,* 2013, **5**, 52–71.

7 Y. Shao, J. Wang, H. Wu, J. Liu, I. A. Aksay and Y. Lin, *Electroanalysis,* 2010, **22**, 1027–36.

8 K. S. Novoselov, A. K. Geim, S. V. Morozov, D. Jiang, Y. Zhang, S. V. Dubonos, I. V. Grigorieva and A. A. Firsov, *Science,* 2004, **306**, 666–669.

9 J. Du, X. Lai, N. Yang, J. Zhai, D. Kisailus, F. Su, D. Wang and L. Jiang, *ACS nano,* 2011, **5**, 590–596.

10 M. A. Rafiee, J. Rafiee, Z. Wang, H. Song, Z. Z.Yu and N. Koratkar, *ACS nano,* 2009, **3**, 3884–3890.

11 B. Thirumalraj, S. Palanisamy, S. M. Chen and B. S. Lou, *J. Colloid Interface Sci.,* 2016, **462**, 375–381.

12 R. Oprea, S. F. Peteu, P. Subramanian, W. Qi, E. Pichonat, H. Happy, M. Bayachou, R. Boukherroub and S. Szunerits, *Analyst,* 2013, **138**, 4345–4352.

13 X. Zhu, Q. Liu, X. H. Zhu, C. Li, M. T. Xu and Y. Liang, *Int. J. Electrochem. Sci*., 2012, **7**, 5172–5184.

14 I. Kaminska, M. R. Das, Y. Coffinier, J. N. Jonsson, P. Woisel, M. Opallo, S. Szunerits, and R. Boukherroub, *Chem. Commun.,* 2012, **48**, 1221–1223.

15 A. Tao, P. Sinsermsuksakul and P. D. Yang, *Nat. Nanotechnol.,* 2007, **2**, 435–440.

16 B. Kong, A. Zhu, Y. Luo, Y. Tian, Y. Yu and G. Shi, *Angew. Chem.,* 2011, **123**, 1877–1880.

17 X. H. Huang, I. H. El-Sayed, W. Qian and M. A. El-Sayed, *Nano Lett.,* 2007, **7**, 1591–1597.

View Article Online
DOI: 10.1039/C6TB01576J

18 M. Schrinner, M. Ballauff, Y. Talmon, Y. Kauffmann, J. Thun, M. Möller and J. Breu, *Science,* 2009, **323**, 617–620.

19 S. Liu, J. Tian, L. Wang, Y. Luo, W. Lu and X. Sun, *Biosens. Bioelectron.,* 2011, **26**, 4491–4496.

20 S. Palanisamy, B. Thirumalraj and S. M. Chen, *RSC Adv.,* 2015, **5**, 94591–94598.

21 F. Y. Kong, Z. Xu, M. T. Xu, J. J. Xu and H. Y. Chen, *Electrochim. Acta,* 2011, **56**, 9386–9390.

22 W. Chen, S. Cai, Q. Q. Ren, W. Wen and Y. D. Zhao, *Analyst,* 2012, **137**, 49–58.

23 S. Palanisamy, H. F. Lee, S. M. Chen and B. Thirumalraj, *RSC Adv.,* 2015, **5**, 105567–105573.

24 Y. Guo, L. Deng, J. Li, S. Guo, E. Wang and S. Dong, *ACS Nano,* 2011, **5**, 1282–1290.

25 Y. Guo, J. Li and S. Dong, *Sens. Actuators, B,* 2011, **160**, 295–300.

26 R. Jiang, D. T. Tran, J. McClure and D. Chu, *Electrochem. Comm.,* 2012, **19**, 73–76.

27 C. J. Gu, F. Y. Kong, Z. D. Chen, D. H. Fan, H. L. Fang and W. Wang, *Biosens. Bioelectron.,* 2016, **78**, 300–307.

28 H. Song, Y. Ni and S. Kokot, *Anal. Chim. Acta,* 2013, **788**, 24–31.

29 J. Chen, L. Zhao, H. Bai and G. Shi, *J. Electroanal. Chem.,* 2011, **657**, 34–38.

30 F. Y. Kong, W. W. Li, J. Y. Wang, H. L. Fang, D. H. Fan and W. Wang, *Anal. Chim. Acta,* 2015, **884**, 37–43.

31 H. L. Zou, B. L. Li, H. Q. Luo and N. B. Li, *Sens. Actuators, B,* 2015, **207**, 535–541.

32 W. S. Hummers and R. E. Offeman, *J. Am. Chem. Soc.,* 1958, **80**, 1339–1339.

33 D. Li, M. B. Mueller, S. Gilje, R. B. Kaner and G. G. Wallace, *Nat. Nanotechnol*., 2008, **3**, 101–105.

34 S. Stankovich, D. A. Dikin, R. D. Piner, K. A. Kohlhaas, A. Kleinhammes, Y. Jia, Y. Wu, S. T. Nguyen and R. S. Ruoff, *Carbon,* 2007, **45**, 1558–1565.

35 I. Calizo, A. A. Balandin, W. Bao, F. Miao and C. N. Lau, *Nano Lett.,* 2007, **7**, 2645–2649.

36 K. J. Hae, P. L. Yun, H. J. Mei, S. K. Eun, J. B. Jung and H. L. Young, *Chem. Phys. Lett*., 2009, **470**, 255–258.

37 Q. Wang, Z. Zhou, D. Chen, J. Lin, F. Ke, G. Xu and S. Sun, *Sci. China Chem.,* 2010, **53**, 2057–2062.

View Article Online
DOI: 10.1039/C6TB01576J

38 J. Zhang, X. Liu, L. Wang, T. Yang, X. Guo, S. Wu, S. Zhang and S. Wang, *Carbon,* 2011, **49**, 3538–3543.

39 Q. Ma, S. Ai, H. Yin, Q. Chen and T. Tang, *Electrochim. Acta,* 2010, **55**, 6687–6694.

40 G. Q. Shi and H. Ohno, *J. Electroanal. Chem.,* 1991, **314**, 59–69.

41 A. J. Bard and L. R. Faulkner, ISBN: 978-0-471-04372-0.

42 J. Chen, U. Wollenberger, F. Lisdat, B. Ge and F. W. Scheller, *Sens. Act. B,* 2000, **70**, 115–120.

43 V. Mani, B. Dinesh, S. M. Chen and R. Saraswathi, *Biosens. Bioelectron.,* 2014, **53**, 420–427.

44 M. E. G. Lyons, C. A. Fitzgerald and M. R. Smyth, *Analyst,* 1994, **119**, 855–861.

45 R. A. Kamin and G. S. Wilson, *Anal. Chem.,* 1980, **52**, 1198–1205.

46 A. S. Kumar, P. Barathi and K. C. Pillai, *Colloids Surf., A,* 2012, **395**, 207–216.

47 K. P. Lee, A. I. Gopalan and S. Komathia, *Sens. Act. B,* 2009, **141**, 518–525.

48 A. S. Kumar, P. Gayathri, P. Barathi and R. Vijayaraghavan, *J. Phys. Chem. C,* 2012,**116**, 23692−23703.

49 X. Lv and J. Weng, *Sci. Rep.,* 2013, **3**, 3285–3295.

50 H. Cao, X. Sun, Y. Zhang, C. Hu and N. Jia, *Anal. Methods,* 2012, **4**, 2412–2416.

51 W. Huang, Q. Hao, W. Lei, L. Wu and X. Xia, *Mater.Res.Express.,* 2014, **1**, 045601–045617.

52 G. Chang, Y. Luo, W. Lu, X. Qin, A. M. Asiri, A. O. Al-Youbi and X. Sun, *Catal. Sci. Technol.,*2012, **2**, 800–806.

53 R. Ning, W. Lu, Y. Zhang, X. Qin, Y. Luo, J. Hu, A. M. Asiri, A. O. Al-Youbi and X. Sun, *Electrochim. Acta,* 2012, **60**, 13–16.

54 X. Qin, Y. Luo, W. Lu, G. Chang, A. M. Asiri, A. O. Al-Youbi and X. Sun, *Electrochim. Acta,* 2012, **79**, 46–51.

55 X. Qin, W. Lu, Y. Luo, G. Chang and X. Sun, *Electrochem. Comm.,* 2011, **13**, 785–787.

56 S. Liu, J. Tian, L. Wang, H. Li, Y. Zhang and X. Sun, *Macromolecules,* 2010, **43**, 10078–10083

View Article Online
DOI: 10.1039/C6TB01576J

Graphical Abstract

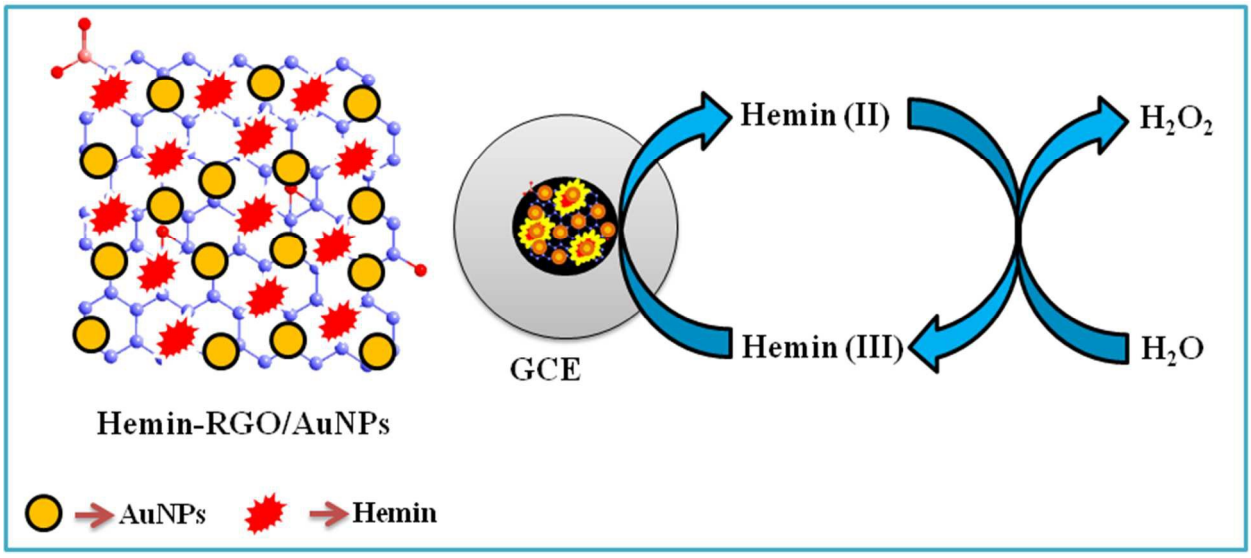

Highlights: Highly stable biomolecule supported AuNPs assisted with graphene nanocomposite as a sensing platform for H_2O_2 biosensor application